JOURNAL OF SOLID STATE CHEMISTRY 6, 169–177 (1973)

Point Defects in Reduced Strontium Titanate*

HISAO YAMADA† AND G. R. MILLER

University of Utah, Salt Lake City, Utah 84112

Received February 29, 1972

Strontium titanate single crystals have been carefully reduced at temperatures ranging from 1200 to 1400°C in oxygen partial pressures of 10^{-7}–10^{-12} atm and quenched to room temperature where optical absorption coefficients, Hall coefficients, mass densities and lattice parameters were measured. (Optical absorption coefficients and Hall coefficients were also measured at 77 K). The predominant defects at room temperature were found to be doubly ionized oxygen vacancies and conduction band electrons. No evidence was found for singly ionized oxygen vacancies as has been suggested by some workers.

Optical absorption in the visible and ultraviolet frequency region was found to be dependent upon the concentration of free carriers. For photon energies of 0.5 eV to about 1 eV, a free carrier absorption effect occurs which may be due to intraband transitions. Three peaks occur at photon energies of 1.66, 2.44, and 2.95 eV and may be due to phonon assisted interband transitions among the titanium *d*-like conduction bands.

Introduction

In recent years, strontium titanate has attracted much attention, both experimental and theoretical, due to its many and varied properties, including superconductivity (*1–3*), second order structural phase transition (*4*) and stress induced phase transition (*5*). Many studies have been directed toward the semiconducting behavior of reduced strontium titanate, including electrical and optical measurements. It is this latter work on which we focus our attention.

The reports of many workers on the electrical and optical properties (*6–20*) of reduced strontium titanate have focused mainly on the properties themselves and not on the relationship between crystal preparation–characterization and these properties. Authors allude occasionally to the point-defects present in reduced strontium titanate without completely characterizing those defects. An example is the use of oxygen vacancy traps in explaining optical data when in fact the existence of oxygen traps has not been proved.

Walters and Grace (*21*) report a study of carefully characterized $SrTiO_3$ at high temperatures where they found that upon reduction of $SrTiO_3$, each oxygen vacancy formed is neutralized by two conduction band electrons. One is prone to think from this work that at lower temperature, these oxygen vacancies could well trap one or more of the conduction band electrons. Certainly the traps would have to be rather shallow, since some researchers (*14, 15*) have found that the Hall coefficient of reduced strontium titanate is constant from 1.2 K to ambient. Only Lee et al. (*17*) have found a temperature dependent Hall coefficient, but the condition of their samples is not clear.

In this study we report results of Hall coefficients, mass density and optical measurements on carefully prepared and characterized reduced strontium titanate in order to classify the situation regarding the point-defects and electron traps.

Experimental

Specimen Preparation

Single crystals of $SrTiO_3$ were obtained from National Lead Company and were annealed in air in a silicon carbide furnace to reduce strains. All samples were packed with $SrTiO_3$ powder. The heating schedule was as follows: The temperature was raised to 1400°C using a heating rate of 300°C/hr, kept at 1400°C for 12 hr, cooled

* Work supported by a grant from the Office of Naval Research, Arlington, VA.

† Present Address: Department of Materials Science and Engineering, Cornell University, Ithaca, NY 14850.

to 500°C at a rate of 50°C/hr and then left in the furnace to cool to room temperature within the furnace. The annealed specimens were then cut into slices perpendicular to the growth axis with a diamond-impregnated wire saw. Specimen thicknesses ranged from 0.5 to 2.5 mm depending on subsequent treatments. All specimens were polished by 0.5 μm Al_2O_3 powder on Teflon-coated grinding wheels.

Reduction heat treatment was carried out in a hydrogen–molybdenum furnace designed for quenching samples from high temperatures to ambient in less than 1 minute. Also in the furnace was a ZrO_2:15% CaO solid state galvanic cell with air reference for oxygen partial pressure measurement. A schematic of the furnace is shown as Fig. 1. Temperature control was to within ±2°C over a 5-hr period. Oxygen pressures in the furnace were controlled by passing O_2 balanced N_2 gas, CO, and CO_2 mixtures or Ar gas through (Ti or Zr) getter-material at high temperatures. After reduction treatment, samples were quenched by dropping to the water-cooled furnace bottom. Etching of the specimens was accomplished in 85% H_3PO_4 at 100°C where etching rates of about 1μm per minute are possible. Normally about 30μm of sample surface was removed. The etching process proved to be rather important since surface reoxidation occurs rapidly even when the sample is quenched to ambient in less than 30 sec.

Hall Constants

Hall constants were measured using a standard dc three-probe technique at room temperature and 77 K. The Hall voltage was measured with a Biddle–Gray six-dial guarded potentiometer and a magnetic field of 10 kG was generated in a 7-in. electromagnet.

The specimens were cut and polished into parallelepiped shapes of 1 × 3 × 10 mm dimensions. Hall and resistivity probes were produced by first drilling $\frac{1}{4}$mm diam, $\frac{1}{2}$ mm deep holes in the sample sides with an airbrasive unit and filled with high-purity indium. Tungsten probes were then pressed into the indium providing good contact. Current contacts were accomplished by covering the sample ends with a 1:1 mixture of indium and Leeds and Northrup thermal free solder.

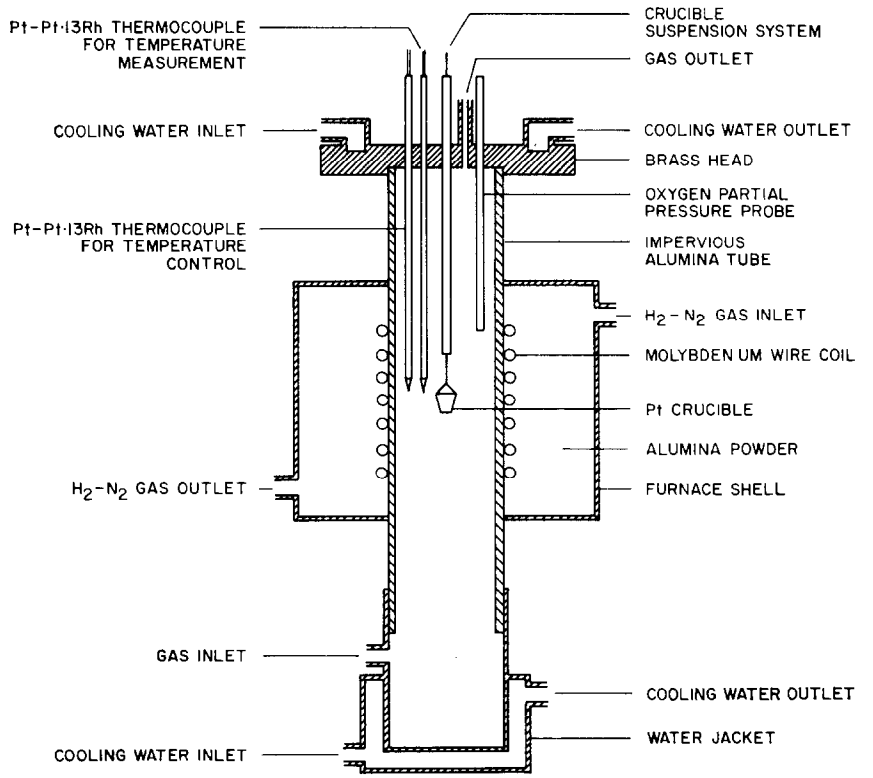

FIG. 1. Schematic of furnace for heat treatment of $SrTiO_3$ samples.

Mass Densities

The method of hydrostatic weighing was selected to accurately determine the densities of the samples and has been described in detail by Smakula (*22*). With the balance used in this equipment along with sample volumes of about 0.2 cm^3, an accuracy of ± 1 part in 10^4 was possible.

Lattice Parameters

Sample lattice parameters were determined using the Debye–Scherrer powder technique on a General Electric XRD-5 diffractometer assembly. Bragg reflections from the (321), (411), (420), (332), and (422) planes were used to determine the lattice parameters. In all cases, an extrapolation of lattice parameter to $\cos^2\theta = 0$ was made via a least-squares analysis.

Optical Densities

Optical densities of specimens were measured in the wavelength range of 0.38–2.6 μm using a Cary 14 spectrophotometer. Corrections for surface reflections were made either by direct subtraction using Bonds (*23*) refraction indices or by varying the sample thickness. Data were taken at 296 and 77 K.

Results

Hall Constants

Hall constants, electron mobilities at 296 and 77 K along with free-carrier densities are listed in Table I. Carrier densities were calculated assuming that

$$n = 1/R_H e \tag{1}$$

where n, R_H, and e are free electron density, Hall constant, and electronic charge, respectively. A plot of free electron densities as a function of oxygen partial pressure at temperatures of 1200–1400°C is shown in Fig. 2. Least-square analyses were performed assuming that the free electron densities are related to oxygen partial pressure by a power law with exponent n. The solid lines in the figure depict the results with n varying from -0.155 to -0.170. Dashed lines are drawn corresponding to best fits to the data with n fixed at $-\frac{1}{6}$. This exponent is predicted from the following quasichemical reaction

$$O_O^* \rightarrow \tfrac{1}{2}O_2(g) + V_O^{2+} + 2e', \tag{2}$$

where O_O^*, V_O^{2+} and e' are oxygen ions at normal sites, doubly ionized oxygen vacancies, and conduction band electrons.

Free electron densities at constant oxygen partial pressures of 10^{-8}, 10^{-9}, 10^{-10}, and 10^{-11} atm (obtained from Fig. 2) are plotted as a function of reciprocal absolute temperature in Fig. 3. Again least-squares analyses were performed giving reaction enthalpies [Eq. (2)] of 5.51, 5.60, 5.77, and 6.07 eV per oxygen vacancy with an experimental uncertainty of ± 0.2 eV. Heat treatment summaries for each sample are given in Table II.

TABLE I

HALL CONSTANTS, ELECTRON MOBILITIES, AND ELECTRON DENSITIES

Sample no.	R_H(cm^3/C)	n(electrons/cm^3)	μ($cm^2 \cdot V^{-1} \cdot sec^{-1}$) at 295 K	μ($cm^2 \cdot V^{-1} \cdot sec^{-1}$) at 77 K
407	2.50	2.5×10^{18}	6.3	2.6×10^2
408	1.60	3.9×10^{18}	5.6	2.3×10^2
409	1.04	6.0×10^{18}	5.9	
410	0.57	1.1×10^{19}	6.1	
401	1.56	4.0×10^{18}	6.4	
402	1.12	5.6×10^{18}	6.1	
404	0.63	1.0×10^{19}	6.5	
405	0.42	1.5×10^{19}	5.8	
301	0.92	6.8×10^{18}	6.1	
304	0.65	9.6×10^{18}	6.2	
305	0.39	1.6×10^{19}	5.4	
306	0.22	2.8×10^{19}	6.3	2.3×10^2
307	0.45	1.4×10^{19}	6.5	
308	0.25	2.5×10^{19}	6.2	
309	0.15	4.1×10^{19}	5.4	
310	0.11	5.8×10^{19}	6.3	

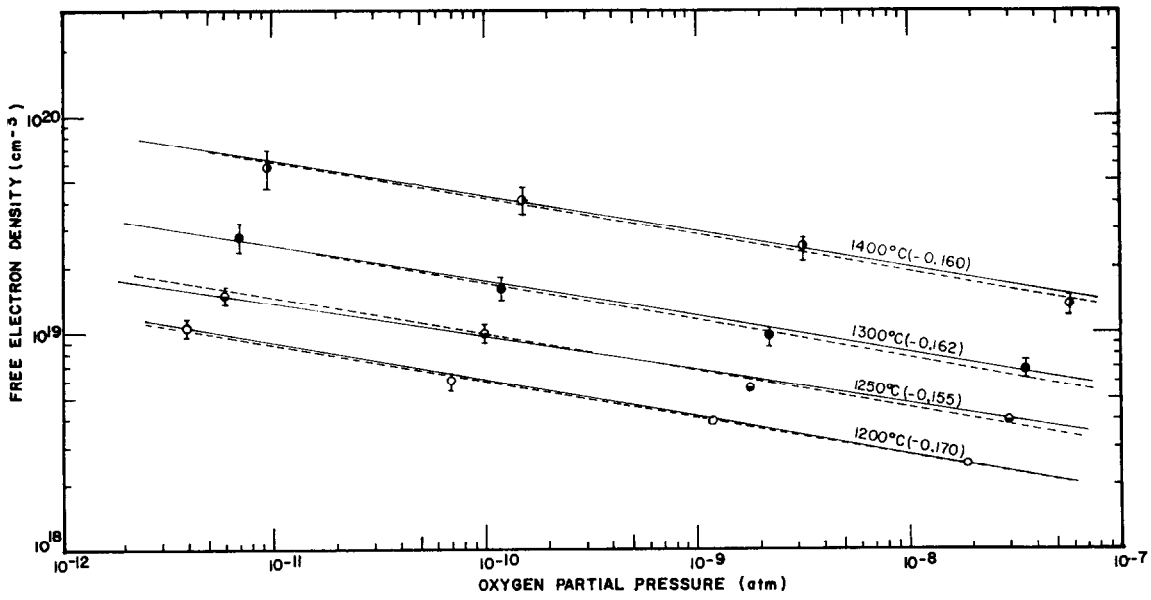

FIG. 2. Free-carrier density as a function of oxygen partial pressure at various temperatures.

Mass Densites

Mass densities determined after annealing and heat treatment are listed in Table III. In order to directly determine vacancy concentrations from density readings, absolute mass densities are needed. However, we found that annealed specimens taken from different single-crystal boules exhibited different densities; hence a comparison of absolute density differences is impossible. Therefore, density differences after annealing and after heat treatment are compared along with those densities calculated from Hall constants assuming the validity of Eq. (2) and no volume change upon reduction. The results are

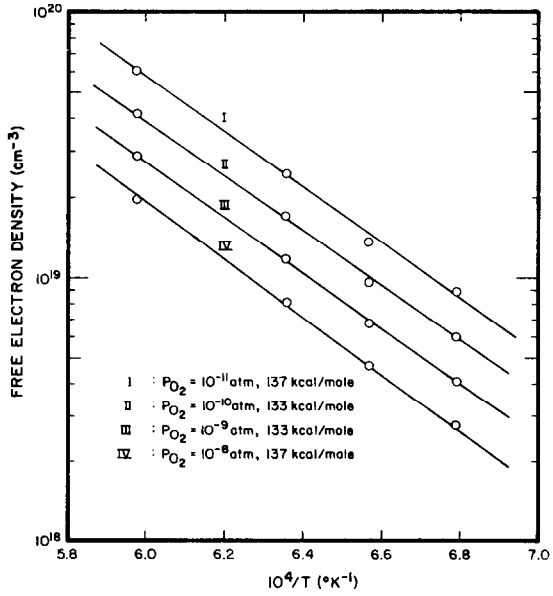

FIG. 3. Free carrier density as a function of reciprocal temperature at various oxygen partial pressures.

TABLE II

SPECIMEN HEAT TREATMENT

Sample no.	Temperature (°C)	Oxygen partial pressure (atm)	Time (hr)
407	1200	2.0×10^{-8}	10
408	1200	1.2×10^{-9}	10
409	1200	7.0×10^{-11}	10
410	1200	4.0×10^{-12}	10
401	1250	3.0×10^{-8}	5
402	1250	1.8×10^{-9}	5
404	1250	1.0×10^{-10}	5
405	1250	6.0×10^{-12}	5
301	1300	3.5×10^{-8}	5
304	1300	2.2×10^{-9}	5
305	1300	1.2×10^{-10}	5
306	1300	7.0×10^{-12}	5
307	1400	5.8×10^{-8}	5
308	1400	3.4×10^{-9}	5
309	1400	1.5×10^{-10}	5
310	1400	9.6×10^{-12}	5

TABLE III

MASS DENSITIES, LATTICE PARAMETERS AND COMPARISON OF OBSERVED AND CALCULATED DENSITY CHANGES

Sample no.	Density after annealing (g/cm^3)	Density after heat treatment (g/cm^3)	Observed density change (g/cm^3)	Calculated density change (g/cm^3)	Lattice parameter (Å)
407	5.1212	5.1212	0.0000	4.0×10^{-5}	3.9047
408	5.1212	5.1212	0.0000	6.0×10^{-5}	3.9052
409	5.1212	5.1211	0.0001	9.0×10^{-5}	3.9051
410	5.1212	5.1211	0.0001	1.6×10^{-4}	3.9050
401	5.1212	5.1212	0.0000	6.0×10^{-5}	3.9051
402	5.1212	5.1211	0.0001	8.0×10^{-5}	3.9049
404	5.1212	5.1211	0.0001	1.5×10^{-4}	3.9048
405	5.1212	5.1210	0.0002	2.2×10^{-4}	3.9050
301	5.1211	5.1210	0.0001	1.0×10^{-4}	3.9049
304	5.1211	5.1210	0.0001	1.4×10^{-4}	3.9047
305	5.1211	5.1209	0.0002	2.4×10^{-4}	3.9048
306	5.1211	5.1207	0.0004	4.2×10^{-4}	3.9049
307	5.1211	5.1209	0.0002	2.1×10^{-4}	3.9053
308	5.1211	5.1207	0.0004	3.7×10^{-4}	3.9049
309	5.1211	5.1205	0.0006	6.1×10^{-4}	3.9051
310	5.1211	5.1203	0.0008	8.6×10^{-4}	3.9053

listed in Table III and are plotted as Fig. 4. A straight line with unit slope is drawn to show the prediction of Eq. (2).

Lattice Parameters

The last column of Table III shows the results of lattice parameter measurements. No significant expansion or contraction of the lattice was observed to the accuracy of our experiments (±0.0005 Å). Since the accuracy of the lattice parameters is not sufficient compared with that of mass densities, no volume change upon reduction was assumed.

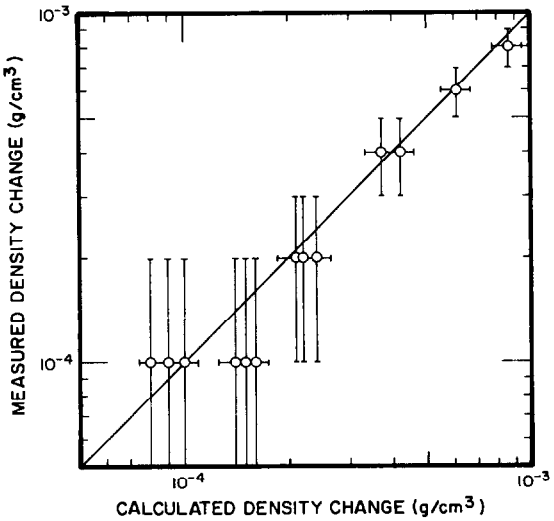

FIG. 4. Comparison of measured and calculated density changes.

Optical Densities

Optical absorption coefficients for specimens heated at 1250°C in various oxygen partial pressures are shown in Figs. 5 and 6. In Fig. 5 the measuring temperature was 296 K, and in Fig. 6 the temperature was 77 K. The dashed line represents an extension of the high-wavelength portion of the curves. The optical absorption coefficients for this straight line portion of the curve at three wavelengths at 296 K are plotted as a function of free electron density in Fig. 7. Straight lines with slope unity are drawn. This free carrier portion of the optical data varies with wavelength as $\lambda^{2.17 \pm 0.02}$ at 296 K and $\lambda^{1.66 \pm 0.10}$ at 77 K. In the wavelength region above 2.0 μm the absorption coefficients show deviation from this power law but it is not clear whether this can be attributed to a true property of reduced $SrTiO_3$ or to poor performance of the instrument above 2.0 μm in this high optical density range.

The absorption coefficient in the wavelength region below 1.0 μm deviates strongly from the so-called free carrier absorption straight line behavior both at 296 and 77 K. The absorption at

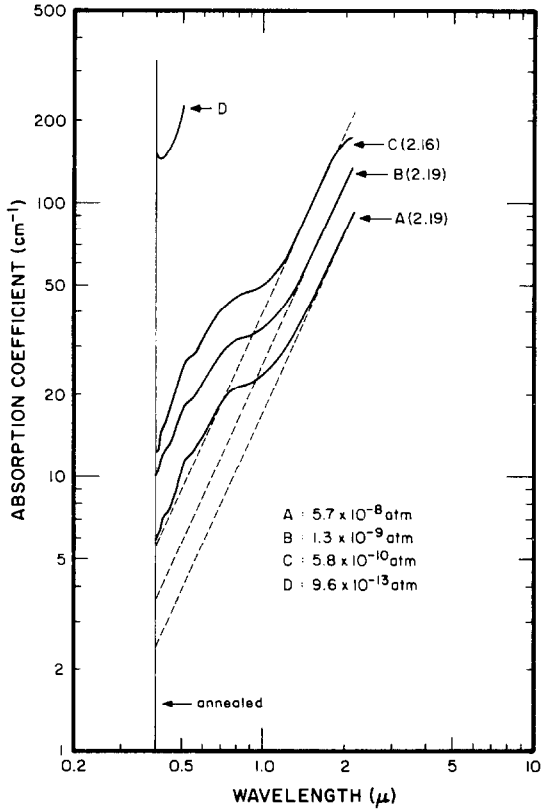

FIG. 5. Optical absorption coefficients at room temperature as a function of photon wavelength for specimen heated at 1250°C in various oxygen partial pressures.

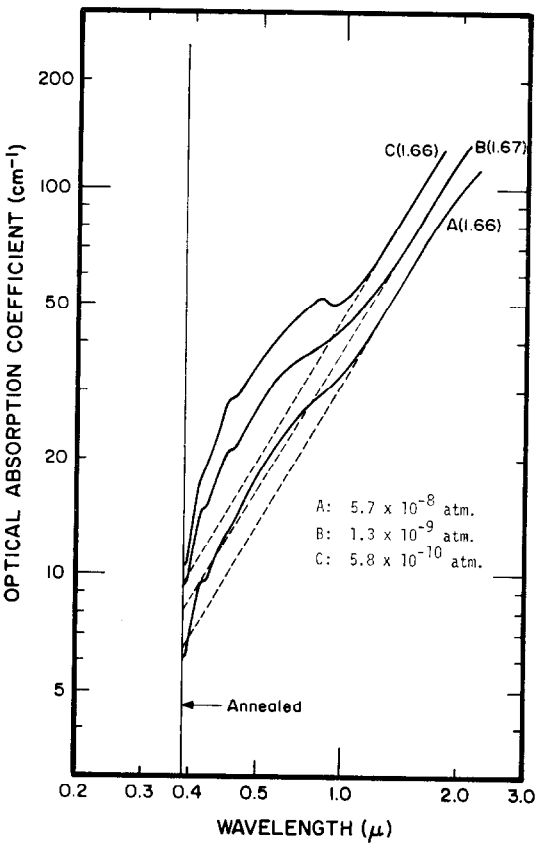

FIG. 6. Optical absorption coefficients at 77 K for specimen heated at 1250°C in various oxygen partial pressures.

296 K over and above the dashed line is plotted in Fig. 8 as a function of photon energy. Three definite peaks can be seen at energies of 1.66, 2.44, and 2.95 eV. All peaks increase with reduction, i.e., with carrier densities, independent of reduction temperature. There is a small change in peak height in going to 77 K, but is considered to be well within experimental and graphical subtraction errors.

Discussion

Based on the fact that the free-electron densities depend on the minus one-sixth power of oxygen partial pressure and that the measured density changes have nearly one-to-one correspondence to the calculated density changes, it is clear that the predominant defects at high temperature can be expressed by the quasi-chemical reaction (2) and, most important, preserved during quenching. The average enthalpy for forming an oxygen vacancy with two conduction band electrons is 5.76 ± 0.20 eV.

Walters and Grace (*21*) obtained an enthalpy of 3.71 eV for the reaction

$$H_2(g) = H_2O(g) + V_O^{2+} + 2e', \qquad (3)$$

from conductivity measurements performed only at the temperature of heat treatment in damp hydrogen mixtures. Their reaction is actually composed of our reaction (2) and the formation of water vapor. Hence the enthalpy of water vapor formation would be added to their value giving an enthalpy for reaction (2) of 6.22 eV, close to the results from our study of quenched samples. One should note that since we have used Eq. (1) for obtaining charge carrier concentrations instead of including the effect of an electron scattering term correction, our interpretations thus far would be in error. Actually, Baer (*18*) has shown that for longitudinal optical phonon scattering by the highest frequency mode in $SrTiO_3$, our Eq. (2) should be corrected to about 16%. In fact, any such error simply shifts our data by 16%, giving no change in slope.

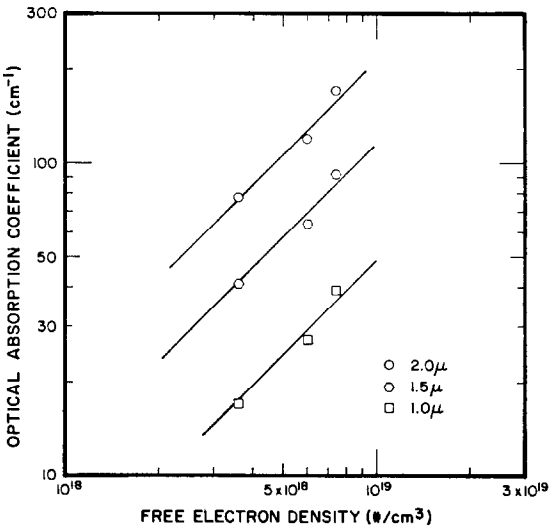

FIG. 7. Optical absorption coefficients at room temperature as a function of free-carrier density.

We wish to comment here on the magnitude of free-carrier densities obtained in this work at reduction temperatures above 1000°C and with oxygen pressures less than 10^{-8} atm. Several workers (*14*, *15*, *17*) have heat treated $SrTiO_3$ specimens in forepump vacuum at temperatures as low as 500°C and yet reached carrier densities as high as those in this experiment. We feel that these discrepancies can be attributed to the fact that oxygen partial pressures calculated from vacuum gauge readings may be orders of magnitude higher than actual oxygen partial pressures, especially at elevated temperatures, because of the presence of impurities such as metal getters and oils from pumps. We have also found that, as may be expected, volumetric ratio measurements of $CO:CO_2$ may not be an accurate indication of oxygen partial pressure due to a lack of attainment of thermodynamic equilibrium. Our studies certainly recommend the solid state cell as a pressure probe. A final comment on the thermodynamics of this system concerns the packing of samples with mixtures of $SrTiO_3$ and TiO_2 powders. Our reasoning for such procedures arose from a desire to fix a third thermodynamic variable besides temperature and oxygen partial pressure. By operating our system at an equilibrium point corresponding to $SrTiO_3$ saturated with TiO_2, we felt that we could always return to a fixed composition. However, since Ti^{4+} and Sr^{2+} ions diffuse so slowly in $SrTiO_3$ as compared with O^{2-}, we never observed a change in composition due to diffusion of cations.

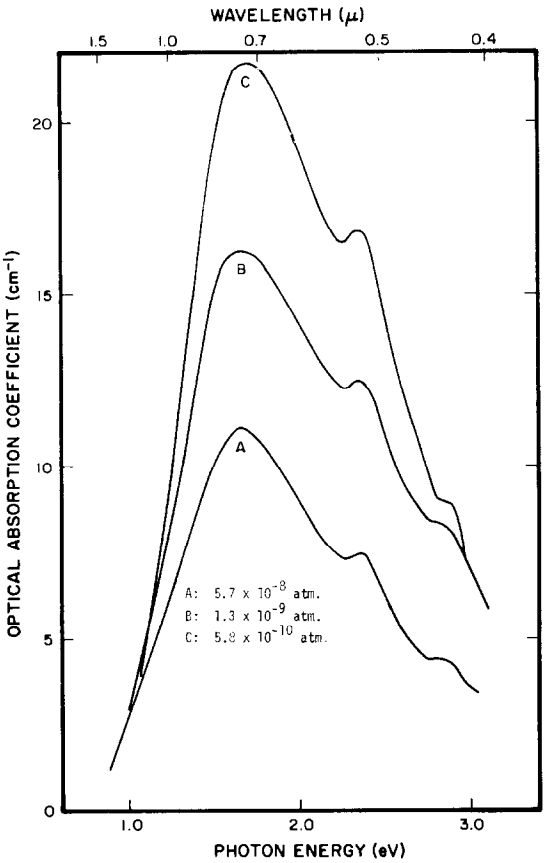

FIG. 8. Optical absorption coefficients obtained by subtracting linear portion of free-carrier absorption (at room temperature).

Since we have shown that oxygen vacancies are doubly ionized at all temperatures down to 77 K and, using other researcher's data, down to 1.2 K, we do not expect any optical absorption to be due to oxygen traps; at least not for photon energies in the range of our measurement.

In the wavelength region of 0.4–2.0 μm, the observed optical absorption is primarily due to free carriers because the absorption increases nearly linearly with free-carrier density. We will discuss the absorption in two parts: (a) the straight line portion of the curves in the wavelength region 1.2–2.2 μm, and (b) the peaks in the curves in the wavelength region 0.4–1.2 μm.

The wavelength dependence of free carrier absorption in a semiconductor can, in principle, be used to determine the scattering mechanism dominant at a given temperature. For completely free electrons, the classical Drude theory, for instance, will predict a λ^2 dependence for free-carrier absorption. Several authors have calcu-

lated the wavelength dependence of absorption due to intravalley electron scattering from acoustical phonons (*24*, *25*), longitudinal optical phonons (*24*, *26*, *27*), and ionized impurity centers (*24*, *28*). The equations resulting from these calculations have been primarily applied to wide conduction-band materials typified by germanium and the III-V semiconductors. A summary of the wavelength dependence predicted by these authors is as follows: (i) For acoustical phonon scattering, $\lambda^{1.5-2.0}$; (ii) For longitudinal optical phonon scattering, $\lambda^{1.5-2.5}$; and (iii) Impurity scattering, $\lambda^{3.0}$. In this study, the absorption data between 1.2 and 2.0 μm at room temperature are best fitted by a $\lambda^{2.2}$ dependence, while at liquid nitrogen temperatures the data are best fitted with a $\lambda^{1.7}$ dependence. Thus it is not immediately clear which scattering mechanism predominates, and in fact a shift in the dominant mechanism may take place. To complicate matters further, it is not obvious that the intravalley scattering mechanism is valid for $SrTiO_3$. It seems that net absorption due to this process of photon absorption with simultaneous photon emission (or absorption) cannot take place for photon energies greater than a conduction bandwidth. For strontium titanate, the conduction bandwidth arising from a single *d* level is quite small (<1 eV) as determined from the Kahn and Leyendecker (*29*) calculation or from effective mass experiments (*14*). Yet Baer (*18*) found a constant wavelength dependence to energies of the order of 2.5 eV. Without observing a peak in this quasi free-carrier absorption effect, one might be tempted to ascribe the effect as the tail of the plasma edge. However, in this material with about 10^{18} electrons/cm^3, the plasma edge should be placed well out in the infrared region (near 100 μm). Thus, it is difficult to imagine this absorption effect to be the plasma tail.

A further model could involve interband absorption since several high effective-mass conduction bands are present in this solid. The interband transition(s) must be phonon assisted since direct transitions are not allowed. Such a mechanism would give little temperature dependence to the absorption curves. This latter observation arises from the fact that the longitudinal optical phonon energies are as high as 0.1 eV and are thus greater than 4 kT at 77 K and roughly equal to 4 kT at 295 K. Thus, spontaneous phonon emission process with no temperature dependence could predominate.

To briefly summarize this point, the mechanism for this quasi free-carrier absorption phenomenon is not clear. If one can, by some stretch of imagination, assume that intravalley scattering predominates, still one can not determine the scattering mechanism. Since a change in wavelength dependence is found between 77 and 295 K, one might assume that the scattering mechanism changes from longitudinal optical phonon interactions at 295 K to acoustical phonons at 77 K. However, this is pure speculation at this point. One can only say with confidence that no optical data exist which show a $\lambda^{3.0}$ dependence indicative of ionized impurity scattering.

Our last point on this subject area centers about the optical absorption data for $SrTiO_3$ obtained by Baer. He reported a $\lambda^{(2.5 \pm 0.1)}$ dependence in the free carrier region of his spectra. His study indicated no significant change in scattering mechanism in the temperature range 77–295 K in contrast to this work.

He also observed a deviation of absorption coefficient from the simple power-law dependence in the wavelength region above 2.5 μm and explained this deviation as due to correction terms in the theoretical work of Gurevich et al. (*27*) which is based upon longitudinal optical phonon-scattering and predicts the $\lambda^{2.5}$ dependence he observed. This correction term includes $(1 - \lambda/\lambda_1)^{1/2}$ where λ_1 is the wavelength of the highest energy longitudinal optical phonon. This term, if one tries to fit his data, is far too weak in its wavelength dependence. For slightly reduced samples in this study and also that of Gandy (*13*), a definite peak centered at about 1.4 μm was found (carrier concentrations less than 10^{18}/cm^3). It is felt that this peak exists "on top of" the free carrier absorption at higher carrier densities; hence, the "bending over" of Baer's data at high wavelength is possibly due to this unexplained peak and not due to deviations from the simple power law he used.

Three absorption peaks were found in the absorption data at 295 and 77 K (Fig. 9). Gandy observed an absorption peak at 2.9 eV and Baer observed an absorption peak at 2.4 eV. They attributed these peaks as due to excitation of electrons trapped at oxygen vacancies, i.e., F_1 centers, but their conclusions seem unreasonable because:

(1) The observed mass density changes were found to be consistent with the calculated mass density changes with an assumption that the predominant defects in reduced strontium titanate are doubly ionized oxygen vacancies with

two conduction-band electrons for each oxygen vacancy formed.

(2) Hall constants of reduced strontium titanate were found to be almost constant from room temperature to 1.2 K by several workers (*14*, *15*, *17*). This indicates that almost all oxygen vacancies are doubly ionized even at 1.2 K. Hence the presence of electrons trapped at an oxygen vacancy at room temperature is negligible. If not negligible, a strong temperature dependence in absorption coefficient should be observed in this wavelength range.

Since the intensity of the three peaks remains essentially unchanged at 295 and 77 K and the intensity of the peaks increases with an increase in free electron density above $10^{18}/cm^3$, the absorption peaks cannot be attributed to excitation of electrons trapped at *another kind* of impurity center. If the absorption peaks are due to excitation of electrons trapped at other impurity centers, one should see a saturation effect in the peak intensity. This is because the concentration of such impurity centers in single-crystal $SrTiO_3$ specimens used in this study is less than $10^{18}/cm^3$. A very probable mechanism for the absorption peaks is that of interband absorption. Since there are several very flat conduction bands in the calculated electron energy bands (*29*), transitions from one conduction band to another conduction band are quite likely in $SrTiO_3$ based on arguments involving a high joint density of states. These transitions must be phonon assisted with probably little or no temperature dependence because spontaneous emission processes may predominate. Evidence for phonon-assisted transitions in $SrTiO_3$ at energies near the conduction band edge has been found by Cappizzi et al. (*10*).

Summary

By rather direct measurements on carefully characterized reduced strontium titanate, we have shown that the oxygen vacancies formed upon reduction can be quenched in upon cooling to ambient and that they remain doubly ionized to very low temperatures. Thus no oxygen vacancy trap for electrons exists and may not be used as a model for optical absorption peaks in the band gap. Rather we propose that such peaks are probably phonon-assisted interband transitions.

References

1. J. E. Schooley, W. R. Hosler, and M. L. Cohen, *Phys. Rev. Lett.* **12**, 474 (1964).
2. J. E. Schooley, W. R. Hosler, E. Ambler, J. H. Becker, M. L. Cohen, and C. S. Koonce, *Phys. Rev. Lett.* **14**, 305 (1965).
3. C. S. Koonce, M. L. Cohen, J. E. Schooley, W. R. Hosler, and E. R. Pfeiffer, *Phys. Rev.* **163**, 380 (1967).
4. P. A. Fleury, J. F. Scott, and J. M. Worlock, *Phys. Rev. Lett.* **21**, 16 (1968).
5. T. S. Chang, J. S. Holzrichter, G. F. Imbusch, and A. L. Schawlow, *Solid State Comm.* **8**, 1179 (1970).
6. O. N. Tufte and E. L. Stelzer, *Phys. Lett.* **141**, 675 (1966).
7. J. A. Noland, *Phys. Rev.* **94**, 724 (1954).
8. S. B. Levin, N. J. Field, F. M. Plock, and L. Merker, *Phys. Rev.* **45**, 737 (1955).
9. M. I. Cohen and R. F. Blunt, *Phys. Rev.* **168**, 929 (1968).
10. M. Capizzi and A. Frova, *Phys. Rev. Lett.* **25**, 1298 (1970).
11. H. P. R. Frederikse, W. R. Hosler, and W. R. Thurber, *Phys. Rev.* **143**, 648 (1966).
12. M. Cardona, *Phys. Rev.* **140**, A651 (1965).
13. H. W. Gandy, *Phys. Rev.* **113**, 795 (1959).
14. O. N. Tufte and P. W. Chapman, *Phys. Rev.* **155**, 796 (1967).
15. H. P. R. Frederikse and W. R. Hosler, *Phys. Rev.* **161**, 822 (1967).
16. D. Parker and J. Yahia, *Phys. Rev.* **169**, 605 (1968).
17. C. Lee, J. Yahia, and J. L. Brebner, *Phys. Rev. B* **3**, 2525 (1971).
18. W. S. Baer, *Phys. Rev.* **144**, 734 (1966).
19. S. H. Wemple, M. DiDomenico, Jr., and A. Jayaraman, *Phys. Rev.* **180**, 547 (1969).
20. H. P. R. Frederikse, W. R. Thurber, and W. R. Hosler, *Phys. Rev. A* **134**, 442 (1964).
21. L. C. Walters and R. E. Grace, *J. Phys. Chem. Solids* **28**, 239 (1967).
22. A. Smakula *in* "Methods of Experimental Physics," (Bederson and Flite, Eds.), Vol. 6A, p. 289. Academic Press, New York (1959).
23. W. L. Bond, *J. Appl. Phys.* **36**, 1674 (1965).
24. H. J. G. Meyer, *Phys. Rev.* **112**, 298 (1958).
25. R. Rosenberg and M. Lax, *Phys. Rev.* **112**, 843 (1958).
26. S. Visvanathan, *Phys. Rev.* **120**, 376 (1960).
27. V. L. Gurevich, I. G. Lang, and Yu. A. Firsov, *Sov. Phys. Solid State* **4**, 918 (1962).
28. S. Visvanathan, *Phys. Rev.* **120**, 379 (1960).
29. A. H. Kahn and A. J. Leyendecker, *Phys. Rev. A* **135**, 1321 (1964).